SUPPORTING INFORMATION

Crystal, electronic, and magnetic structures of M_2AgF_4 (M = Na – Cs) phases as viewed from the DFT+U method

Dominik Kurzydłowski, Mariana Derzsi, Zoran Mazej and Wojciech Grochala

Table of contents

I. Details of the magnetic coupling calculations

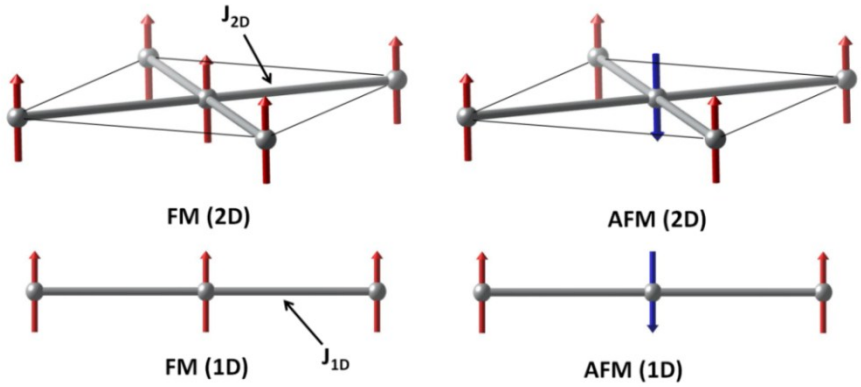

Fig. S 1 Spin states of a 2D square lattice and 1D symmetric chain.

For the layered perovskite phases the super-exchange-mediated magnetic coupling within the $[AgF_{4/2+2}]^{2-}$ square layers (J_{2D}) can be calculated with the use of the broken-symmetry method. Taking the Heisenberg Hamiltonian in the form of $^{H_{ij}} = -J_{ij}s_is_j$ one can express the energies of the FM(2D)/AFM(2D) spin states (Fig. S 1) in terms of J_{2D}, as shown in Table S 1. In analogy, the magnetic coupling constant within the $[AgF_{4/2+2}]^{2-}$ chains of PP can be calculated with the knowledge of the energies of the FM(1D)/AFM(1D) states.

Table S 1 Relations between the energy of a given spin state and the magnetic coupling constants (J_{1D}/J_{2D})

System	Energy per spin*	*J* value	Ground state
1D	$E_{FM} = -¼J_{1D} + E$ $E_{AFM} = ¼J_{1D} + E$	$J_{1D} = 2\cdot(E_{AFM} - E_{FM})$	FM ($J_{1D} > 0$) AFM ($J_{1D} < 0$)
2D	$E_{FM} = -½J_{2D} + E$ $E_{AFM} = -½J_{2D} + E$	$J_{2D} = E_{AFM} - E_{FM}$	FM ($J_{2D} > 0$) AFM ($J_{2D} < 0$)

* where E is the spin-independent part of the total energy.

We note that as a result of the tilting distortions present in AE_β and FC_β these phases should be characterized by two types of super-exchange routes between nearest-neighbor Ag(II) centers (Ag-F2a-Ag and Ag-F2b-Ag, as shown in Fig. S 2). Therefore the J_{2D} values calculated as described above are in fact a mean of two coupling constants (J_{2D}' and J_{2D}") characterizing each coupling route. We note though that the sign of these coupling constants should be the same as J_{2D}, and their values similar. This is supported by calculations on the FC_β phase of K_2AgF_4 which yields J_{2D}' = –22.5 meV, J_{2D}" = –11.3 meV, hence average J_{2D} = –16.9 meV.

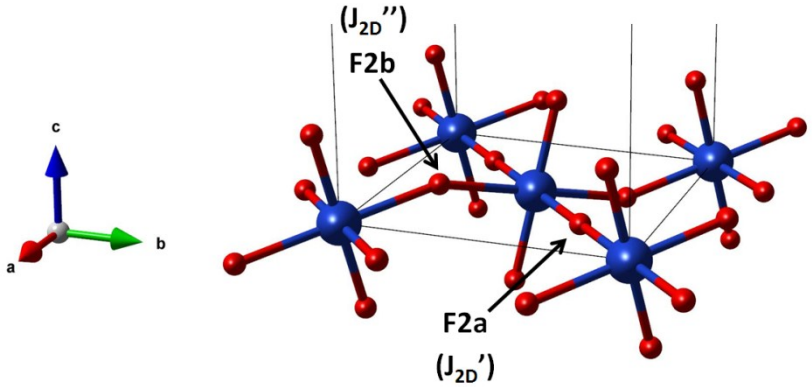

Fig. S 2 Influence of the β-type tilts on the 2D superexchange pathway.

II. Mapping the potential surface between HT- (*Bmab*) and LT-K_2AgF_4 ($P2_1/c$) with DFT+U

Computational details Using a linear-combination approach we have generated 10 model structures to map the potential surface between HT (α, of *Bmab* symmetry) and LT (β, of $P2_1/c$ symmetry) polymorphs of K_2AgF_4. The former structure form was first transformed to the LT representation with a transformation matrix (-1 0 0, 0 -1 0, 1 0 1) (Fig. S 3). Consequently, the structure parameters (coordinates and lattice vectors) of the two polymorphs were linearly combined as xHT + (1-x)LT for 10 values of x with step equal to 0.1. Such constructed models were fully optimized considering both ferromagnetic and antiferromagnetic ordering. The DFT and spin-polarized DFT+U calculations were performed in the VASP package with the DFT+U method and a plane-wave cut-off equal to 800 eV. Only results of magnetic calculations are discussed, as nonmagnetic calculations result in wrong ground state (see Fig. S 5).

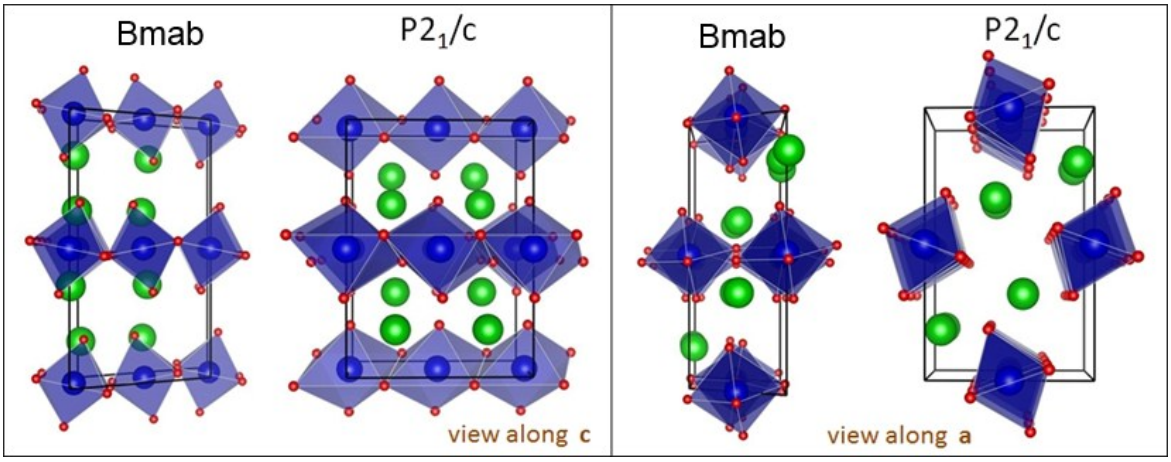

Fig. S 3 Unit cell of HT- and LT-K_2AgF_4 used as starting structures for generation of 10 model structures via linear combination approach. The HT form is visualized in a LT ($P2_1/c$) representation.

Results

Main structural changes along HT → LT transformation path All obtained structures are visualized in Fig. S 4. The important structural changes along the HT → LT transformation path account for change in the AgF_6 octahedra and their orbital ordering pattern. First, the contracted AgF_6 octahedron changes to elongated one and simultaneously the ferrodistortive ordering pattern of $d(x^2\text{-}y^2)$ orbitals along the **ab** plain changes to antiferrodistortive one (x=0.1–0.4). Next, the $d(x^2\text{-}y^2)$ orbitals reorient in such a way as to form parallel stacking that propagates along **a** axis (x=0.5). Such stacking leads to considerable reduction of the LT angle by 20^O. These features (the parallel stacking and LT angle approaching 90^o) are reminiscent of the LT polymorph with the exception that the potassium atoms are not located at the central positions of the van der Waals cavities between the AgF_6 octaherda. Respective shifts in the potassium sub-lattice enforce a butterfly coordination around Ag atoms and it take place for x=0.6. Once the potassium atoms are shifted the parallel stacking of the $d(x^2\text{-}y^2)$ orbitals recovers and the LT polymorph is stabilized (x =0.7 – 0.9).

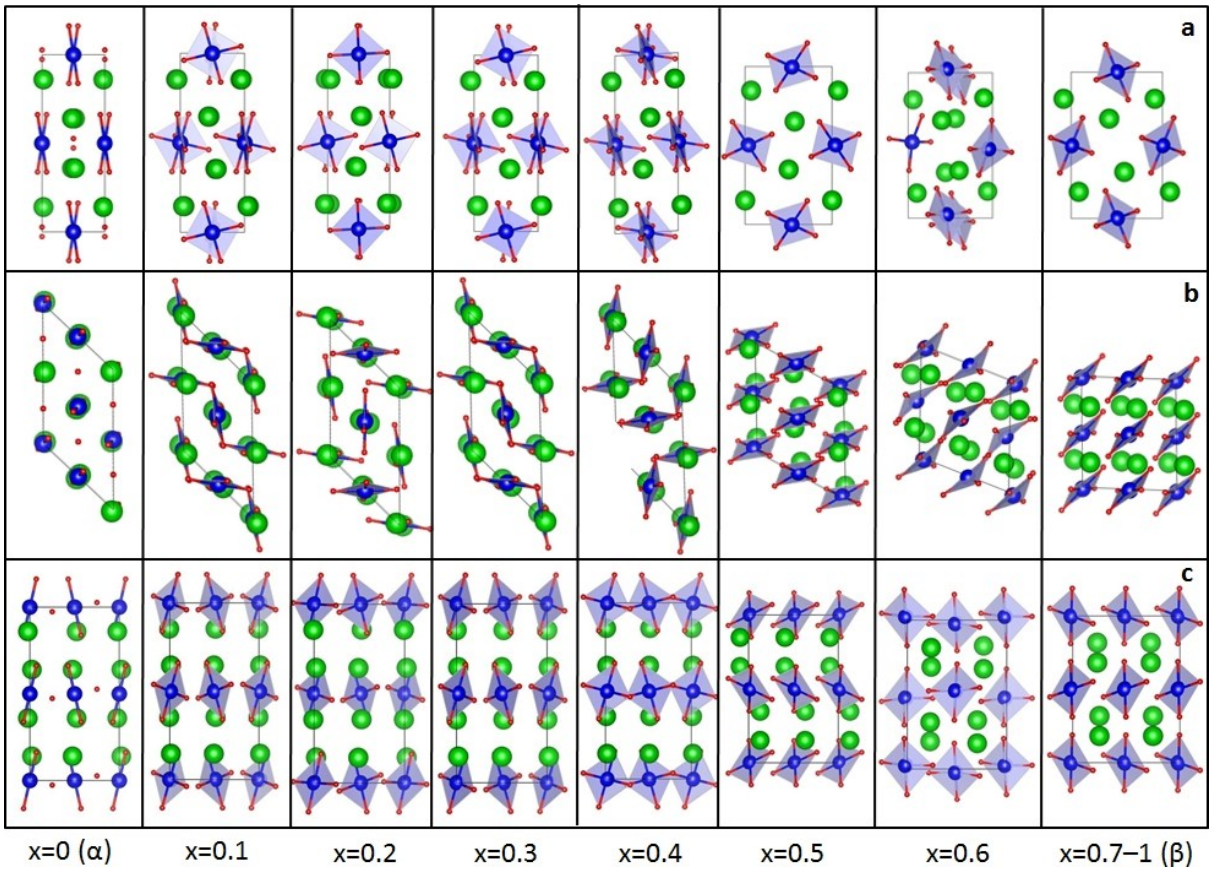

Fig. S 4 All optimized ferromagnetic models shown along axes a **(top),** b **(middle) and** s **(bottom) of the LT-K_2AgF_4 representation.**

Energy barrier along HT → LT transformation path The energy barrier calculated for ferromagnetic models is shown in Fig. S 5. Change of the contracted AgF_6 octahedron to

elongated one and simultaneous change of the ferrodistortive ordering pattern of $d(x^2-y^2)$ orbitals to the antiferrodistortive one amounts for large energy decrease by 180 meV/FU (x=0 → x=0.1). This transition is another indication of the tendency for K_2AgF_4 to adopt the AE-type arrangement in the layered perovskite structure. The elongated octahedra and the antiferrodistortive ordering is preserved in following three structures (x=0.2-0.4) which differ in energy maximally by 40 meV/FU. These order of magnitude smaller energy changes can be assigned to slight changes in relative tilting of the AgF_6 octahedra. The perovskite type structures are separated from the LT polymorph by an energy barrier of 180 meV/FU, which accounts mainly for changes in potassium sub-lattice.

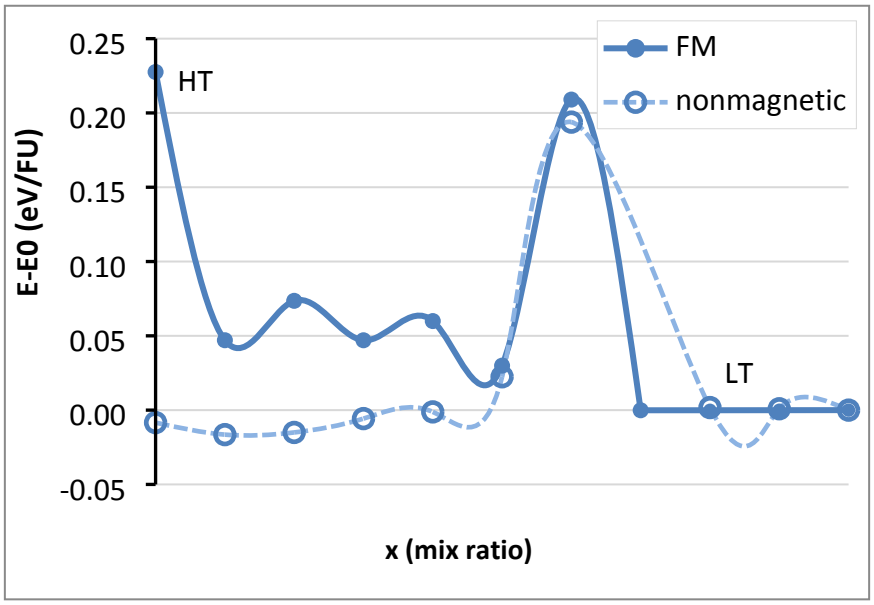

Fig. S 5 Energy barrier between HT (*Bmab*) and LT ($P2_1/c$) polymorphs calculated for nonmagnetic and FM models. Note that the true barrier height may differ from that calculated for x=0.6.

Generally speaking, all linear combinations of HT and LT polymorphs resulted in AE and PP types of structures.

In order to obtain more detailed information about the potential energy surface of the perovskite and post-perovskite forms of K_2AgF_4 we have additionally calculated a monoclinic variants of the *Bmab* structure (FM $C2/c$ and AFM $P2_1/c$), another variant with infinite linear AgF chains (AFM $P4_2mc$), post-perovskite structure with contracted AgF_6 octahedra and the contraction taking place along the direction of the octahedral stacking (Pbam) and finally perovskite structure with ideally flat AgF_2 layers considering both contracted and elongated ocrahedra (FM $I4/mmm$ and AFM $C2/c$). The analysis presented below focuses on general trends considering also these additional polymorphs.

Coordination / Jahn-Teller distortions Structures with 2+2+2 and 4+2 (with both elongated and contracted octahedra) coordination were obtained. In all structures with 2+2+2 coordination, the difference between the two sets of equatorial Ag-F distances is maximally 0.06 Å, while the difference between axial and equatorial distances is usually by one order of magnitude larger. The amount of the distortion $d(Ag\text{-}F)_{eq}/d(Ag\text{-}F)_{ax}$ translates to energetic stabilization of the structures - the energy decreases with the increase of the octahedral distortion (Figure 4). The distortion is the largest for elongated octahedra (0.44–0.70) and it is considerably smaller for contracted octahedra (0.06–0.32). In consequence, the solutions with contracted octahedra are separated from the solutions with elongated octahedra by 100 meV/FU gap. There is one solution that strongly deviates from this linear trend in Fig. S 6. This is a *C*2/c cell with 2D AFM ordering. Its high energy suggests that the 2D AFM ordering is substantially disfavoured (see below).

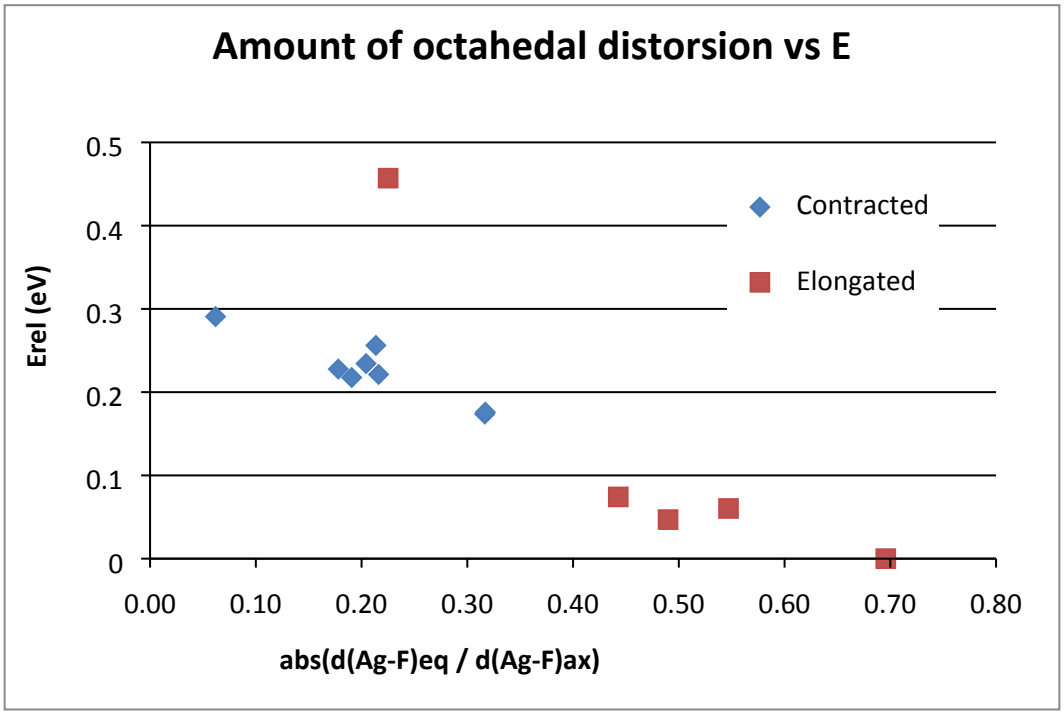

Fig. S 6 Energy of all calculated K_2AgF_4 models plotted as a function of an amount of octahedral distortion calculated as $d(Ag\text{-}F)_{eq}$ / $d(Ag\text{-}F)_{ax}$, where $d(Ag\text{-}F)_{eq}$ stands for average equatorial Ag-F distance and $d(Ag\text{-}F)_{ax}$ for average axial Ag-F distance.

Orbital ordering In all obtained structures, the relative orientation of the nearest-neighbour highest-occupied *d* orbitals is such as to minimize their overlap. Thus, in structures with elongated AgF_6 octahedra the highest occupied $d(x^2\text{-}y^2)$ orbitals exhibit antiferrodistortive ordering and in the structures with contracted AgF_6 octahedra, the highest occupied dz^2 orbitals exhibit parallel ordering. In structures with antiferrodistortive ordering of the magnetic $d(x^2\text{-}y^2)$ orbitals, the extremely large JT distortion ($abs(d(Ag\text{-}F)_{eq}/d(Ag\text{-}F)_{ax}) > 0.44$) that controls their separation prevents stabilization of the AFM solution.

Table S 2 List of all calculated K_2AgF_4 models ordered in respect to their increasing relative energy dE=E-E_0. For each structure orbital ordering pattern (OO) and Ag-F distances are listed. AE = **antiferrodistortive ordering of elongated octahedra.** FC = **ferrodistortive ordering of contracted octahedra.** PP-E **– post-perovskite with elongated octahedra.** PP-C **– post-perovskite with contracted octahedra.**

mag	symm	dE	OO	Ag-F1	Ag-F2	Ag-F3
FM 1D	*P*2$_1$/c (LT)	0.000	PP-E	2.130	2.112	2.816
FM 2D	*P*bca	0.047	AE	2.130	2.120	2.615
FM 2D	*P*-1 no.1	0.060	AE	2.124	2.123	2.670
FM 2D	*P*-1 no.2	0.074	AE	2.120	2.138	2.571
FM 1D	*P*bam	0.174	PP-C	2.395	2.395	2.078
AFM 1D	*P*bam	0.176	PP-C	2.395	2.395	2.078
FM	*C*2/c	0.218	FC	2.307	2.285	2.105
AFM 2D	*P*2$_1$/c (from *C*2/c)	0.221	FC	2.324	2.289	2.091
FM	*Bmab* (HT)	0.228	FC	2.286	2.286	2.108
AFM 2D	*P*2$_1$/c (from *C*mca)	0.234	FC	2.295	2.299	2.093
AFM 2D	*P*42mc	0.256	FC	2.339	2.278	2.095
FM	*I*4/mmm	0.291	FC	2.217	2.217	2.155
AFM 2D	*C*2/c (from *I*4/mmm)	0.457	FE	2.125	2.125	2.350

III. References

1. G. A. Baker, H. E. Gilbert, J. Eve, and G. S. Rushbrooke, *Phys. Lett. A*, 1967, **25**, 207.
2. G. A. Bain and J. F. Berry, *J. Chem. Educ.*, 2008, **85**, 532.
3. Z. Mazej, E. Goreshnik, Z. Jagličić, B. Gaweł, W. Łasocha, D. Grzybowska, T. Jaroń, D. Kurzydłowski, P. J. Malinowski, W. Koźmiński, J. Szydłowska, P. J. Leszczyński, and W. Grochala, *CrystEngComm*, 2009, **11**, 1702.